28. D. King, J. Roughgarden, *Theor. Popul. Biol.* **21**, 194 (1982).
29. D. Cohen, *J. Theor. Biol.* **12**, 119 (1966).
30. D. King, J. Roughgarden, *Theor. Popul. Biol.* **22**, 1 (1982).
31. P. Haccou, Y. Iwasa, *Theor. Popul. Biol.* **47**, 212 (1995).
32. E. Kussell, S. Leibler, *Science* **309**, 2075 (2005).
33. L. Watson, M. J. Dallwitz, *The Families of Flowering Plants: Descriptions, Illustrations, Identification, and Information Retrieval.* Version: 29 July 2006 http://delta-intkey.com (1992 onward).
34. T. Keller, J. Abbott, T. Moritz, P. Doerner, *Plant Cell* **18**, 598 (2006).
35. A. C. Whibley *et al.*, *Science* **313**, 963 (2006).
36. S. Gavrilets, *Fitness Landscapes and the Origin of Species*, S. Levin, H. Horn, Eds., Monographs in Population Biology (Princeton Univ. Press, Princeton and Oxford, 2004).
37. We thank J. Avondo for help with visualizing 3D fitness landscapes, M. Clauss for helpful discussions on bet-hedging, and C. Thébaud for advice on inflorescence databases. This research was funded by grants from Human Frontier Science Program (E.C. and P.P.), Natural Sciences and Engineering Research Council of Canada (P.P. and L.H.), and the Biotechnology and Biological Sciences Research Council, UK (E.C.).

Supporting Online Material
www.sciencemag.org/cgi/content/full/1140429/DC1
Materials and Methods
SOM Text
Fig. S1
References
SOM Programs

25 January 2007; accepted 30 April 2007
Published online 24 May 2007;
10.1126/science.1140429
Include this information when citing this paper.

Marine Radiocarbon Evidence for the Mechanism of Deglacial Atmospheric CO_2 Rise

Thomas M. Marchitto,[1,2]*† Scott J. Lehman,[1,2]* Joseph D. Ortiz,[3] Jacqueline Flückiger,[2]‡ Alexander van Geen[4]

We reconstructed the radiocarbon activity of intermediate waters in the eastern North Pacific over the past 38,000 years. Radiocarbon activity paralleled that of the atmosphere, except during deglaciation, when intermediate-water values fell by more than 300 per mil. Such a large decrease requires a deglacial injection of very old waters from a deep-ocean carbon reservoir that was previously well isolated from the atmosphere. The timing of intermediate-water radiocarbon depletion closely matches that of atmospheric carbon dioxide rise and effectively traces the redistribution of carbon from the deep ocean to the atmosphere during deglaciation.

Radiocarbon measurements of calendrically dated hermatypic corals (*1*) and planktonic foraminifera (*2*, *3*) indicate that the radiocarbon activity ($\Delta^{14}C$) of the atmosphere during the latter part of the last glacial period [~20,000 to 40,000 years before the present (yr B.P.)] ranged from ~300 to 800 per mil (‰) higher than it was during the prenuclear modern era (Fig. 1C). Although reconstructions of Earth's geomagnetic-field intensity predict higher cosmogenic ^{14}C production rates during the glacial period, production was apparently not high enough to explain the observed atmospheric enrichment (*2*–*5*). Rather, a substantial fraction of the atmosphere's $\Delta^{14}C$ buildup must have been due to decreased uptake of ^{14}C by the deep ocean. This requires a concomitant ^{14}C depletion in a deep-ocean dissolved inorganic C reservoir that was relatively well isolated from the atmosphere. Renewed ventilation of this reservoir could theoretically explain the drop in atmospheric $\Delta^{14}C$ (Fig. 1C) and the rise in atmospheric CO_2 (*6*) across the last deglaciation. Most workers point to the Southern Ocean as a locus of deglacial CO_2 release, based on the similarity between atmospheric CO_2 and Antarctic temperature records (*6*) and on numerous conceptual and numerical models (*7*–*9*). If correct, we would expect some signature of the low-^{14}C deep-ocean C reservoir to be spread to other basins via Antarctic Intermediate Water (AAIW). Here, we report a strong radiocarbon signal of the deglacial release of old C, recorded in an intermediate-depth sediment core from the northern edge of the eastern tropical North Pacific.

Intermediate water $\Delta^{14}C$ reconstruction. Marine sediment multi-core/gravity-core/piston-core triplet from sediment layer MV99-MC19/GC31/PC08 was raised from a water depth of 705 m on the open margin off the western coast of southern Baja California (23.5°N, 111.6°W) (*10*). The site is today situated within the regional O_2 minimum zone that exists because of a combination of high export production and poor intermediate-water ventilation. Various sediment properties in MC19/GC31/PC08 vary in concert with the so-called Dansgaard-Oeschger (D-O) cycles that characterized the Northern Hemisphere climate during the last glacial period (*11*). Originally discovered in Greenland ice cores, D-O cycles also exist in a number of lower-latitude locations that were probably teleconnected to the North Atlantic region through the atmosphere (*2*, *12*, *13*). Off the coast of Baja California, the sedimentary concentrations of organic C, Cd, Mo, and benthic foraminifera all decreased sharply during D-O stadials (cold periods in Greenland) (*11*, *14*). Together, these proxies are consistent with reduced productivity during stadials, caused by either decreased coastal upwelling or a deepening of the regional nutricline related to the mean state of the tropical Pacific (*11*).

Diffuse spectral reflectance (DSR) provides a 1-cm resolution stratigraphy for GC31/PC08. After R-mode factor analysis, the third factor of DSR (Fig. 1A) exhibits the strongest correlation to the productivity proxies and to Greenland climate (*11*). We used this DSR record to apply a calendar-age model to MC19/GC31/PC08, based on correlation to $\delta^{18}O$ (an air-temperature proxy) in Greenland ice core GISP2 (Greenland Ice Sheet Project 2) (*15*). Resulting calendar ages were then combined with 50 benthic foraminiferal radiocarbon ages [19 of which were published previously (*10*)] to calculate age-corrected intermediate-water $\Delta^{14}C$ (*16*). To evaluate the partitioning of ^{14}C between the atmosphere and the ocean, we compared intermediate-water $\Delta^{14}C$ to that of the atmosphere (Fig. 1C), as reconstructed from tree rings (*17*), U-Th–dated corals (*1*, *17*), and planktonic foraminifera from Cariaco Basin off Venezuela (*3*). Calendar ages for Cariaco Basin were originally based on the correlation of lithologic climate proxies to the GISP2 $\delta^{18}O$ record (*2*), which has been layer-counted with visual and chemical techniques (*15*). However, Hughen *et al.* (*3*) recently demonstrated that the Cariaco Basin ^{14}C calibration yields much better agreement with coral results older than ~22,000 yr B.P. when an alternate age model is used, based on correlation to the U-Th–dated Hulu Cave speleothem $\delta^{18}O$ record from eastern China (*13*). Because DSR in GC31/PC08 is more similar to the Greenland isotope record than to the lower-resolution Hulu Cave record, we continued to use the GISP2 correlation but applied simple provisional age adjustments to GISP2 older than 23,400 yr B.P., using four tie points to Hulu Cave (Fig. 1B and fig. S1). We do not suggest that this age model is necessarily superior to the original one (*15*), but this exercise is necessary for comparing our data to the most recent (and most consistent) atmospheric $\Delta^{14}C$ reconstructions (*1*, *3*, *17*). The resulting age model for MC19/GC31/PC08, based on 21 tie points, yields a very constant sedimentation rate (fig. S2) and gives us confidence that our calendar-age assignments for ^{14}C samples between tie points are reliable to within a few hundred years (table S1).

Baja California intermediate-water radiocarbon activities are plotted in red in Fig. 1C. The

[1]Department of Geological Sciences, University of Colorado, Boulder, CO 80309, USA. [2]Institute of Arctic and Alpine Research, University of Colorado, Boulder, CO 80309, USA. [3]Department of Geology, Kent State University, Kent, OH 44242, USA. [4]Lamont-Doherty Earth Observatory, Columbia University, Palisades, NY 10964, USA.

*These authors contributed equally to this work.
†To whom correspondence should be addressed. E-mail: tom.marchitto@colorado.edu
‡Present address: Environmental Physics, Institute of Biochemistry and Pollutant Dynamics, Eidgenössische Technische Hochschule Zürich, 8092 Zürich, Switzerland.

Downloaded from www.sciencemag.org on June 7, 2007

modern activity, based on a local seawater measurement of –131‰ at 445 m and the nearest Geochemical Ocean Section Study profile (*18*), is estimated to be –170‰, in good agreement with the core top value. Comparable offsets from the contemporaneous atmosphere were maintained throughout the Holocene (typically ~100‰ between 0 and 10,000 yr B.P.) and during the latter part of the glacial period (roughly 200‰ between 20,000 and 30,000 yr B.P.) (*19*). Radiocarbon activities before 30,000 yr B.P. show increased scatter that may be related to the greater influence of slight contaminations on older samples.

Overall, it is clear that intermediate waters mainly followed atmospheric $\Delta^{14}C$ over the past 40,000 yr, except during the last deglaciation. Activities dropped sharply just after 18,000 yr B.P., reaching minimum values of ~–180‰ between 15,700 and 14,600 yr B.P., roughly 450‰ lower than that of the contemporaneous atmosphere. For comparison, the lowest $\Delta^{14}C$ values found in the modern ocean (in the North Pacific near 2-km water depth) are depleted by ~240‰, relative to the preindustrial atmosphere (*18*). A second comparably large depletion event began sometime between 13,500 and 12,900 yr B.P. and ended between 12,100 and 11,600 yr B.P. The magnitude of ^{14}C depletion we reconstructed during these two deglacial events is much too great to attribute to changes in dynamics of the North Pacific thermocline (*20*) and must instead record a large change in the initial ^{14}C activity of waters advected to the site. Such depleted waters could have been sourced only from the deepest, most isolated regions of the glacial ocean (*21*).

Link to atmospheric history. In Fig. 2, we compare the timing of reconstructed intermediate-water and atmospheric $\Delta^{14}C$ changes with the deglacial record of atmospheric CO_2 from the East Antarctic Dome C ice core (*6*). The latter is shown on a GISP2 layer-counted time scale based on a simple synchronization of CH_4 variations between the Dome C and GISP2 ice cores (supporting online material text and table S2). It is immediately apparent that the atmospheric $\Delta^{14}C$ decline and CO_2 rise occurred in parallel, with a synchronous, intervening plateau appearing in both records. There is a slight (and still unreconciled) difference in the timing of the start of the deglacial atmospheric $\Delta^{14}C$ decline between the Cariaco Basin (*3*) and IntCal04 (*17*) reconstructions, but we take the deglacial onset of the atmospheric CO_2 rise and the atmospheric ^{14}C decline to be essentially synchronous. We now also find that these changes were associated with a prominent decline in $\Delta^{14}C$ of intermediate water in the eastern North Pacific that must record the redistribution of aged C from the deep ocean to the surface. After 14,600 yr B.P., intermediate-water activities rebounded to higher values, coincident with the plateau in both the atmospheric CO_2 rise and the atmospheric $\Delta^{14}C$ drop. The leveling of the atmospheric records and the increase in ^{14}C activity of intermediate waters are all indicative of a reduction in the flux of aged C to the upper ocean and atmosphere from below. After ~12,800 yr B.P., the atmospheric CO_2 rise and $\Delta^{14}C$ drop resumed, and intermediate-water activities again reached minimum values of ~–180‰, indicating a resumption of C redistribution from the deep ocean to the surface. By 11,500 yr B.P., the large deglacial atmospheric shifts were mostly completed, and intermediate-water activities finally reached modern values.

As pointed out by Monnin *et al.* (*6*), the deglacial rise of atmospheric CO_2 closely followed the rise in East Antarctic temperatures (Fig. 3A), implying that the ocean's release of C to the atmosphere was associated with changes in the Southern Ocean. Deep convection of the Southern Ocean both ventilates much of the ocean interior and returns to the atmosphere much of the C extracted by photosynthesis in the sunlit surface of the global ocean. During the last

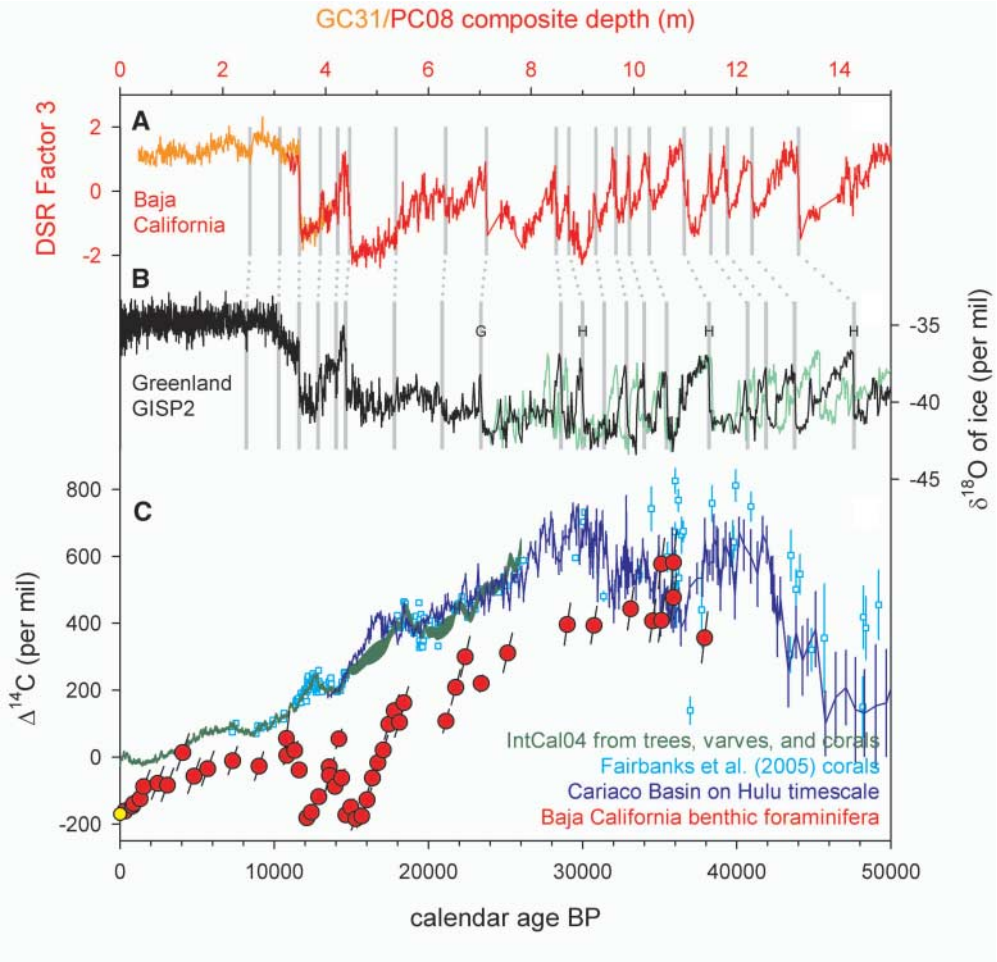

Fig. 1. Intermediate-water and atmospheric $\Delta^{14}C$ records. (**A**) Diffuse spectral reflectance factor 3 from Baja California composite sediment core MV99-GC31/PC08, plotted versus depth (top axis) (*11*). Gray lines show tie points to the Greenland record that were used to derive the calendar-age model. (**B**) $\delta^{18}O$ of Greenland ice core GISP2 (*15*) on a provisional revised time scale (black, bottom axis). The new time scale deviates from the original time scale (green) for calendar ages older than 23,400 yr B.P. (vertical line labeled G). The new time scale is based on linear interpolation between point G and three tie points whose ages are derived from U-Th–dated Hulu Cave (vertical lines labeled H) (*13*). (**C**) Atmospheric radiocarbon activities based on tree rings, planktonic foraminifera from Cariaco Basin varve-counted sediments, and U-Th–dated corals (dark green) (*17*); additional recent coral measurements (light blue) (*1*); and planktonic foraminifera from Cariaco Basin, based on an age model derived from the correlation of sediment reflectance to Hulu Cave (dark blue) (*3*). Red circles show intermediate-water activities from benthic foraminifera in MC19/GC31/PC08. The yellow circle is an estimate for modern bottom waters at this site. Error bars are based on compounded uncertainties in radiocarbon ages and calendar ages.

Downloaded from www.sciencemag.org on June 7, 2007

glacial period, density stratification of the Southern Ocean surface and/or extensive sea-ice coverage are suggested to have isolated deep waters from the atmosphere (*7–9*), permitting the buildup of a larger deep-ocean C reservoir and a consequent drawdown of atmospheric CO_2. Sediment pore water chlorinity and $\delta^{18}O$ measurements, combined with benthic foraminiferal $\delta^{18}O$, indicate that deep Southern Ocean waters were the saltiest and densest waters in the glacial ocean (*22*). Such high salinities point to brine formation beneath sea ice as an important mode of formation. At deglaciation, a progressive renewal of deep convection or upwelling in association with documented sea-ice retreat (*23*) [and possibly with poleward-shifting westerlies (*8*)] would have provided for the simultaneous delivery of ocean heat and sequestered C to the atmosphere. This transition occurred in two major steps, beginning with relatively early (~18,000 years ago) and gradual increases in temperature and CO_2 that were temporarily interrupted by the Antarctic Cold Reversal (ACR). Major transients in our record of $\Delta^{14}C$ in intermediate-depth waters of the eastern North Pacific conform to this Antarctic schedule, consistent with the redistribution of C from the abyss to the upper ocean and atmosphere in connection with changes in deep convection of the Southern Ocean.

$\delta^{13}C$ provides a tracer that is complementary to $\Delta^{14}C$, though with a far smaller dynamic range in seawater. During the last glacial period, the deep Southern Ocean contained the ocean's lowest $\delta^{13}C$ values, suggesting a local accumulation of remineralized C and/or poor ventilation (*24*). Spero and Lea (*25*) argued that during the early part of the last deglaciation, Southern Ocean sea-ice retreat (*23*), combined with increased deep convection and northward Ekman transport, imparted transient low $\delta^{13}C$ values to AAIW and Subantarctic Mode Waters and that this signal was recorded by deep-dwelling planktonic foraminifera in various ocean basins, including the eastern tropical North Pacific. These waters should also have carried a low $\Delta^{14}C$ signature, and we suggest that this is the signal we observe off the coast of Baja California. Today, AAIW is barely traceable as a distinct water mass north of the equator in the eastern tropical Pacific (*26*). We argue that the northward penetration of AAIW during deglaciation was greater than it is today (*27*) and was at times fed by extremely ^{14}C-depleted waters sourced from the abyss by deep overturning in the Southern Ocean. Sea-ice retreat could have allowed the upwelled deep waters to gain buoyancy from precipitation, converting some fraction of these waters into AAIW without substantial mixing with warmer thermocline waters (*28*), which would otherwise dampen the $\Delta^{14}C$ signal. There is evidence that vertical stratification of the North Pacific also varied on an Antarctic climate schedule (*29*), so northern deep waters may have supplemented the supply of aged C to the Baja California site. However,

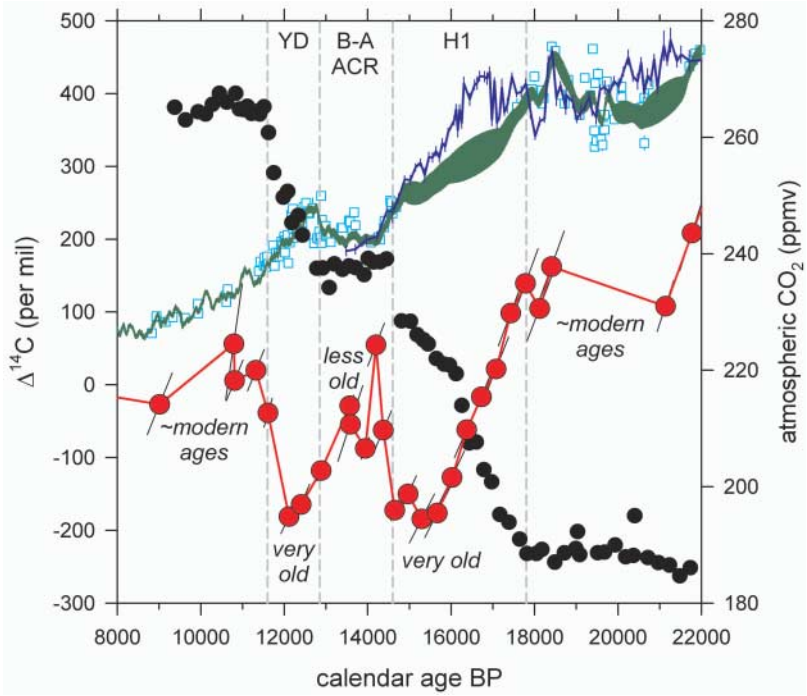

Fig. 2. Baja California intermediate-water $\Delta^{14}C$ during the last deglaciation (red), compared with atmospheric $\Delta^{14}C$ (dark green, light blue, and dark blue) (*1*, *3*, *17*), and atmospheric CO_2 from Antarctica Dome C (*6*) placed on the GISP2 time scale (black), as discussed in the text. Vertical dashed gray lines show the ages of Bølling-Allerød (B-A) and Younger Dryas (YD) boundaries, based on the GISP2 $\delta^{18}O$ record, and the start of Heinrich event 1 (H1), based on the $^{231}Pa/^{230}Th$ record from Bermuda Rise (*34*). The ACR is contemporaneous with the Bølling-Allerød. ppmv, parts per million by volume.

the interaction of strong circumpolar winds with bathymetry in the Southern Ocean provides for much more effective vertical pumping (*30*) than do conditions in the North Pacific, and therefore southern sources probably dominated the $\Delta^{14}C$ changes in our record.

North-south teleconnections. Numerous observational and modeling studies indicate an inverse relationship between Antarctic and North Atlantic temperature variations that may be due to altered interhemispheric ocean-heat transport and/or opposing local deep-water formation histories (*28*, *31–33*). Insofar as $\Delta^{14}C$ of the intermediate-depth Pacific provides an inverse proxy for the strength of deep convection in the Southern Ocean, our results provide strong evidence for tight, inverse coupling of deep-water formation between hemispheres. This is clearly demonstrated by the covariation of intermediate-depth Pacific $\Delta^{14}C$ and the formation history of North Atlantic Deep Water (NADW) [or its glacial analog, Glacial North Atlantic Intermediate Water (GNAIW)], based on measurements of $^{231}Pa/^{230}Th$ from sediments in the western North Atlantic (*34*) (Fig. 3C). The near-cessation of ^{231}Pa export beginning just after 18,000 yr B.P. records a collapse of GNAIW that has been linked to a massive discharge of glacial ice and fresh water to the North Atlantic, known as Heinrich event 1. After a recovery during the Bølling-Allerød warm phase, another marked weakening of NADW/GNAIW is documented during the Younger Dryas cold period, probably also triggered by a discharge of glacial meltwater (*34*). Both periods of NADW/GNAIW reduction were times of intermediate-depth Pacific $\Delta^{14}C$ decline and atmospheric CO_2 rise.

It is often difficult to identify triggers in a tightly coupled system, but the relationships described above suggest that the Antarctic climate schedule may have been paced by ice sheet and meltwater forcing around the North Atlantic. Support for this conclusion comes from our observation that although major inflections in the $\Delta^{14}C$ and $^{231}Pa/^{230}Th$ records in Fig. 3 were almost exactly synchronous, the large $\Delta^{14}C$ decrease (i.e., Southern Ocean ventilation increase) during Heinrich event 1 occurred more gradually than did the associated decrease in GNAIW export. This relationship is consistent with relatively slow circum-Antarctic warming due to anomalous ocean-heat transport (*33*), leading to sea-ice retreat (*23*) [and possibly poleward-shifting westerlies (*8*)] and, consequently, a progressive increase in deep overturning of the Southern Ocean. Alternatively, Southern Ocean overturning may have been instigated by NADW/GNAIW reductions through the requirement (*35*) that global rates of deep-water formation balance global deep upwelling, which is forced mainly by winds and tides. The abrupt rise in atmospheric $\Delta^{14}C$ at the start of the Younger Dryas [+80‰ in just 180 years (*36*)] (Fig. 2) may record the time elapsed before the Southern Ocean could begin respond-

Downloaded from www.sciencemag.org on June 7, 2007

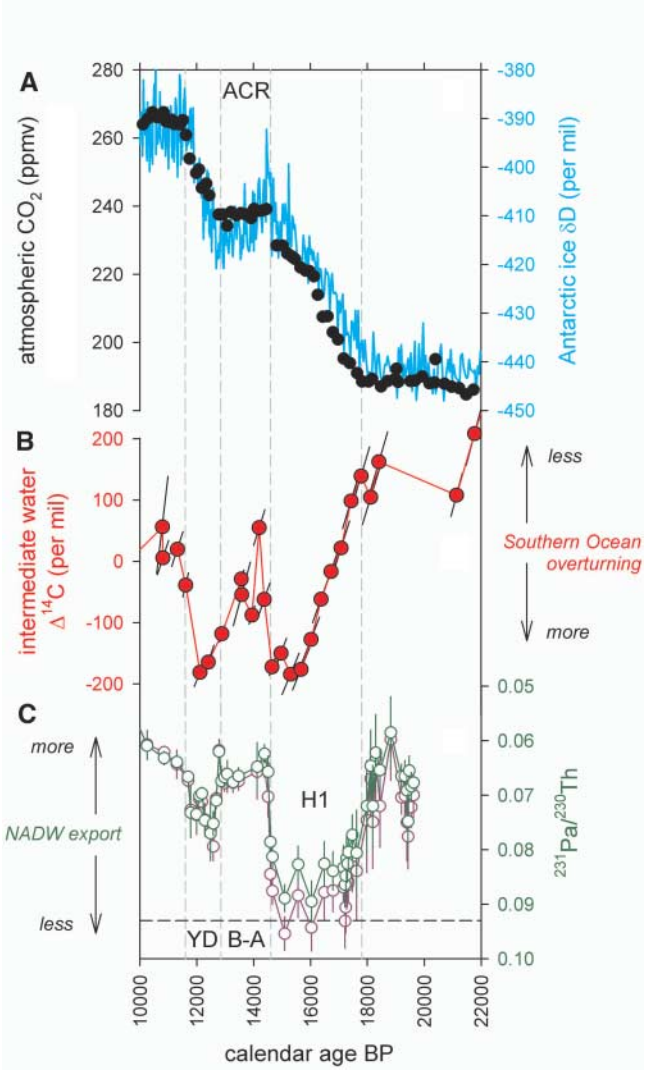

Fig. 3. Southern and northern ocean-atmosphere changes during the last deglaciation, compared with intermediate-water $\Delta^{14}C$. (**A**) Atmospheric CO_2 (black) and ice core deuterium (δD) temperature proxy (light blue) from Antarctica Dome C (*6*), placed on the GISP2 time scale. (**B**) Baja California intermediate-water $\Delta^{14}C$. (**C**) Inverted decay-corrected excess $^{231}Pa/^{230}Th$ in Bermuda Rise sediments, based on two methods to calculate excess (green and purple) (*34*). The horizontal dashed line shows the water-column production ratio for these isotopes (0.093); lower values are primarily due to Pa export by vigorous NADW. Vertical dashed lines show the ages of climatic boundaries, as in Fig. 2. Error bars are based on compound uncertainties in radiocarbon ages and calendar ages.

ing to reduced NADW formation, leading to the brief absence of deep-ocean sinks for ^{14}C (*32*).

Recent work shows that deep North Atlantic radiocarbon activities also increased abruptly during the Bølling-Allerød because of renewed formation of NADW and that they temporarily decreased during the Younger Dryas, when NADW formation was again briefly restricted (*37*, *38*). In light of our new record, this pattern of deep-ocean change was probably limited to the North Atlantic (arising from deep circulation changes within the basin), whereas the intermediate-depth North Pacific record tracks the overall redistribution of C from the deep ocean to the atmosphere.

Implications for the deep C reservoir. Finally, our results bear on recent questions concerning reconstructed rates of atmospheric $\Delta^{14}C$ decline during deglaciation and implied ^{14}C aging of glacial deep waters. Although subject to uncertainties (*19*), decay projection of our first deglacial $\Delta^{14}C$ minimum back to the surface ocean (*39*) gives an apparent ventilation age of ~4000 years, implying that the inferred deep Southern Ocean source waters were at least that old. This is broadly consistent with the minimum deep-ocean age estimated from the atmospheric record, assuming that the old reservoir filled half of the ocean's volume (*40*). Ages of up to 5000 years have been reported for glacial deep waters near New Zealand (*41*), but more northerly sites in the Pacific show little difference from today, at least at depths shallower than ~2 km (*40*). We infer that the greatest ^{14}C depletion of the glacial deep ocean was probably concentrated in the Southern Ocean region (and deepest Pacific), coincident with the highest densities (*22*) and lowest $\delta^{13}C$ values (*24*).

References and Notes

1. R. G. Fairbanks *et al.*, *Quat. Sci. Rev.* **24**, 1781 (2005).
2. K. Hughen *et al.*, *Science* **303**, 202 (2004).
3. K. Hughen, J. Southon, S. J. Lehman, C. Bertrand, J. Turnbull, *Quat. Sci. Rev.* **25**, 3216 (2006).
4. C. Laj *et al.*, *Earth Planet. Sci. Lett.* **200**, 177 (2002).
5. R. Muscheler *et al.*, *Earth Planet. Sci. Lett.* **219**, 325 (2004).
6. E. Monnin *et al.*, *Science* **291**, 112 (2001).
7. D. M. Sigman, E. A. Boyle, *Nature* **407**, 859 (2000).
8. J. R. Toggweiler, J. L. Russell, S. R. Carson, *Paleoceanography* **21**, PA2005 (2006).
9. B. B. Stephens, R. F. Keeling, *Nature* **404**, 171 (2000).
10. A. van Geen *et al.*, *Paleoceanography* **18**, 1098 (2003).
11. J. D. Ortiz *et al.*, *Geology* **32**, 521 (2004).
12. R. J. Behl, J. P. Kennett, *Nature* **379**, 243 (1996).
13. Y. J. Wang *et al.*, *Science* **294**, 2345 (2001).
14. W. E. Dean, Y. Zheng, J. D. Ortiz, A. van Geen, *Paleoceanography* **21**, PA4209 (2006).
15. P. M. Grootes, M. Stuiver, *J. Geophys. Res.* **102**, 26455 (1997).
16. Materials and methods are available as supporting material on *Science* Online. In the supporting material, we also present our $\Delta^{14}C$ values calculated with the original GISP2 chronology (*15*) and compare them to the original Cariaco record (*2*), based on correlation to GISP2 (fig. S3).
17. P. J. Reimer *et al.*, *Radiocarbon* **46**, 1029 (2004).
18. G. Ostlund, H. Craig, W. S. Broecker, D. Spencer, *GEOSECS Atlantic, Pacific and Indian Ocean Expeditions*, vol. 7, *Shorebased Data and Graphics* (U.S. Government Printing Office, Washington, DC, 1987).
19. Throughout most of this paper, we discuss our $\Delta^{14}C$ values with respect to the contemporaneous atmosphere, rather than calculating ventilation ages by decay projection (*39*) because of large uncertainties in initial surface-ocean reservoir ages and the possibility of multiple intermediate- and deep-water sources with different ventilation histories.
20. U. Mikolajewicz, T. J. Crowley, A. Schiller, R. Voss, *Nature* **387**, 384 (1997).
21. The deglacial injection of low-^{14}C intermediate waters along the Baja California margin did not noticeably overprint the DSR or other O_2-sensitive productivity proxies recorded in GC31/PC08. Although $\Delta^{14}C$ and O_2 are broadly correlated in the modern ocean, they can also be decoupled (*18*) through air-sea exchange. Hence, deglacial intermediate waters were very depleted in $\Delta^{14}C$ but apparently not drastically depleted in O_2.
22. J. F. Adkins, K. McIntyre, D. P. Schrag, *Science* **298**, 1769 (2002).
23. R. Gersonde, X. Crosta, A. Abelmann, L. Armand, *Quat. Sci. Rev.* **24**, 869 (2005).
24. U. S. Ninnemann, C. D. Charles, *Earth Planet. Sci. Lett.* **201**, 383 (2002).
25. H. J. Spero, D. W. Lea, *Science* **296**, 522 (2002).
26. P. C. Fiedler, L. D. Talley, *Prog. Oceanogr.* **69**, 143 (2006).
27. S. Schulte, F. Rostek, E. Bard, J. Rullkötter, O. Marchal, *Earth Planet. Sci. Lett.* **173**, 205 (1999).
28. R. F. Keeling, B. B. Stephens, *Paleoceanography* **16**, 112 (2001).
29. S. L. Jaccard *et al.*, *Science* **308**, 1003 (2005).
30. J. R. Toggweiler, B. Samuels, *Deep-Sea Res.* **42**, 477 (1995).
31. T. J. Crowley, *Paleoceanography* **7**, 489 (1992).
32. W. S. Broecker, *Paleoceanography* **13**, 119 (1998).
33. R. Knutti, J. Flückiger, T. F. Stocker, A. Timmermann, *Nature* **430**, 851 (2004).
34. J. F. McManus, R. Francois, J.-M. Gherardi, L. D. Keigwin, S. Brown-Leger, *Nature* **428**, 834 (2004).
35. W. Munk, C. Wunsch, *Deep-Sea Res.* **45**, 1977 (1998).
36. K. A. Hughen, J. R. Southon, S. J. Lehman, J. T. Overpeck, *Science* **290**, 1951 (2000).
37. L. C. Skinner, N. J. Shackleton, *Paleoceanography* **19**, PA2005 (2004).
38. L. F. Robinson *et al.*, *Science* **310**, 1469 (2005).
39. J. F. Adkins, E. A. Boyle, *Paleoceanography* **12**, 337 (1997).
40. W. Broecker *et al.*, *Science* **306**, 1169 (2004).
41. E. L. Sikes, C. R. Samson, T. P. Guilderson, W. R. Howard, *Nature* **405**, 555 (2000).

42. We thank D. Lopez, J. Turnbull, and C. Wolak for laboratory assistance; J. Southon for accelerator mass spectrometry analyses; A. Pearson for providing an unpublished seawater $\Delta^{14}C$ measurement; and T. Blunier for providing Dome C EDC 3 time scale and for valuable discussions on synchronization of the different ice cores. This manuscript was improved by comments from R. Keeling and two anonymous reviewers. Support was provided by NSF grants OCE-9809026 and OCE-0214221.

Supporting Online Material

www.sciencemag.org/cgi/content/full/1138679/DC1
Materials and Methods
SOM Text
Figs. S1 to S3
Tables S1 and S2
References

11 December 2006; accepted 27 April 2007
Published online 10 May 2007;
10.1126/science.1138679
Include this information when citing this paper.

Downloaded from www.sciencemag.org on June 7, 2007

www.sciencemag.org/cgi/content/full/1138679/DC1

Supporting Online Material for

Marine Radiocarbon Evidence for the Mechanism of Deglacial Atmospheric CO_2 Rise

T. M. Marchitto,* S. J. Lehman, J. D. Ortiz, J. Flückiger, A. van Geen

*To whom correspondence should be addressed. E-mail: tom.marchitto@colorado.edu

Published 10 May 2007 on *Science* Express
DOI: 10.1126/science.1138679

This PDF file includes:

Materials and Methods
SOM Text
Figs. S1 to S3
Tables S1 and S2
References

Supporting Online Material

Methods

Bulk sediment samples were washed using a sodium hexametaphosphate solution and picked for benthic foraminifera using the >250 μm size fraction, supplemented with 150-250 μm specimens where necessary. Toward the end of this study, picked foraminifera were also briefly sonicated in methanol (Table S1). Foraminiferal samples were hydrolyzed with H_3PO_4 and reduced to graphite using an Fe catalyst in the presence of H_2. The 19 published radiocarbon samples (*S1*) were graphitized at the National Ocean Sciences AMS Facility in Woods Hole (NOSAMS), while the 31 new samples were graphitized at the INSTAAR Laboratory for AMS Radiocarbon Preparation and Research at the University of Colorado, Boulder (NSRL). All published radiocarbon data (*S1*) were analyzed at NOSAMS, while all new data were analyzed at the Keck Carbon Cycle AMS Facility at the University of California, Irvine (KCCAMS). $\delta^{13}C$ corrections were based on off-line measurement for NOSAMS results, and on measurement within the AMS for KCCAMS results. KCCAMS $\delta^{13}C$ values are not suitable for paleoceanographic interpretation, and are therefore not reported. Age-corrected $\Delta^{14}C$ calculations were based on the conventions of Stuiver and Polach (*S2*). $\Delta^{14}C$ error bars were calculated by compounding radiocarbon age errors with estimated calendar age errors listed in Table S1. Calendar age errors depend solely on the estimated precision of our picks with respect to the GISP2-Hulu chronology, and not on any errors in the GISP2-Hulu chronology itself. The latter would affect both our record and the Cariaco Basin atmospheric $\Delta^{14}C$ record similarly.

Hulu Cave adjustments to GISP2 age model

In order to compare PC08 results with the most recent and most consistent atmospheric $\Delta^{14}C$ reconstructions (*S3*-*S5*), the correlation between PC08 reflectance and GISP2 $\delta^{18}O$ (*S6*) (used to derive calendar ages for calculating PC08 $\Delta^{14}C$) requires that the GISP2 chronology be consistent with the Hulu Cave chronology (*S7*), as outlined in the main text. Younger than ~20-25 kyr BP the Hulu Cave and GISP2 chronologies appear to be consistent with each other, so no corrections need to be applied to the more recent parts of the GISP2 age model (Fig. S1). GISP2 also agrees with the latest NGRIP chronology (GICC05) to within 250 yr over this interval (*S8*). We adjusted the GISP2 chronology older than 23.4 kyr BP (the start of Interstadial 2) by linearly interpolating between three Hulu Cave tie-points corresponding to major interstadial warmings in Greenland. The resulting GISP2 age model appears to agree with Hulu Cave to within a few hundred years throughout the past 50 kyr (Fig. S1). The resulting age-depth relationship for PC08 is shown in Fig. S2A.

Methane synchronization of Dome C and GISP2

As outlined above and in the main text, the GISP2, Hulu Cave, and coral chronologies are similar over the last ~20-25 kyr. However, these chronologies differ from the glaciological age model on which the EPICA Dome C CO_2 and δD records of Monnin *et al*. (*S9*) were originally presented. To obtain a timescale that is consistent with the various $\Delta^{14}C$ reconstructions, we have used CH_4 records from the Dome C, GISP2, and GRIP ice cores (*S9*-*S11*) to derive a GISP2 synchronized gas age scale for Dome C.

Seven tie-points (Table S2) were defined based on the comparison of the Dome C CH_4 record (on the EDC3 time scale (*S12, S13*)) and the GISP2 and GRIP CH_4 records (on the GISP2 time scale (*S10*)). Between the tie-points the EDC3 gas age scale was linearly interpolated to GISP2 ages. The associated ice age scale for Dome C was derived from the synchronized gas age scale described above and the delta ages (gas age to ice age differences in the ice core) taken from the EDC3 time scale (*S12, S13*).

Sedimentary artifacts

The two deglacial intervals of depleted radiocarbon activity that we report appear, in part, as large age plateaus in the conventional radiocarbon age:depth relationship (Table S1). During the first (earlier) event, radiocarbon age is nearly constant over 90 cm of core depth, and during the second event, radiocarbon age is nearly constant over at least 45 cm. Near-instantaneous massive inputs of sediment, namely slumps, could theoretically produce age plateaus. However, such events would necessarily produce large kinked offsets in the calendar age:depth relationship, which are clearly not observed (Fig. S2). Additionally, slumps are much more likely to produce age reversals than plateaus. Radiocarbon age plateaus could also theoretically be created during intervals of very intense bioturbation, such that age is homogenized over some depth interval. However, it is unreasonable to postulate a complete, simultaneous bioturbational homogenization of the upper 90 cm (or 45 cm) of the sediment column, especially in this low-O_2 environment. The entire MC19/GC31/PC08 record is dominated by low-O_2 benthic foraminiferal taxa (mainly *Bolivina* and *Uvigerina*), and sedimentary Mo remains enriched by ~4-8 times crustal values during deglaciation, indicative of shallow pore water sulfide and suboxic bottom waters (*S14*). Finally, very intense bioturbation would homogenize other paleoclimate proxies in this core. Notably, our second age plateau crosses the Allerød-Younger Dryas boundary in GC31/PC08, which is marked by a sharp reflectance change that is inferred to record a shift in surface ocean productivity (*S15*). We therefore conclude decisively that the ^{14}C age-depth patterns in our record reflect changes in intermediate water ^{14}C activity and not sedimentary processes.

Alternate PC08 age model

We have also calculated Baja California $\Delta^{14}C$ based on correlation to GISP2 using the original layer-counted age model of Meese *et al*. (*S16*) (Fig. S3). This record only differs from our preferred GISP2-Hulu age model prior to 23.4 kyr BP. In Fig. S3 we compare this alternate record to the original Cariaco Basin $\Delta^{14}C$ record based on correlation to GISP2 (*S17*). It is clear that our conclusions are not affected by the choice of age model, though the agreement between Cariaco Basin and coral $\Delta^{14}C$ is better in Fig. 1 than in Fig. S3 (*S5*). The PC08 age-depth relationship for the alternate age model is shown in Fig. S2B.

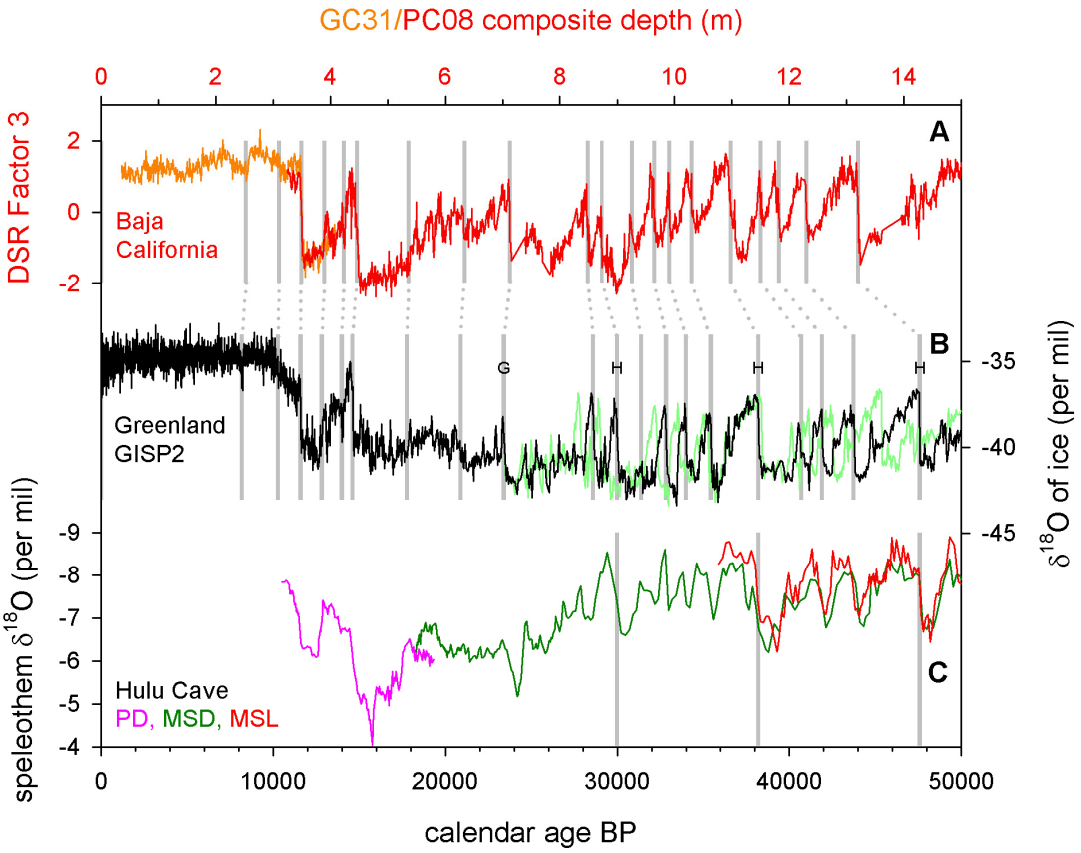

Fig. S1. Derivation of GISP2-Hulu Cave composite age model. (**A**) Diffuse spectral reflectance factor 3 from Baja California composite sediment core MV99-GC31/PC08, plotted versus depth (*S15*). Gray lines show tie-points to Greenland record used to derive calendar age model. (**B**) $\delta^{18}O$ of Greenland ice core GISP2 (*S6*) on provisional revised timescale (black). New timescale deviates from original timescale (green) older than 23.4 kyr BP (line labeled G). New timescale is based on linear interpolation between point G and three tie-points whose ages are derived from U-Th-dated Hulu Cave (lines labeled H). (**C**) Hulu Cave $\delta^{18}O$ from three different stalagmites (*S7*). Gray lines indicate tie-points used to adjust GISP2 chronology.

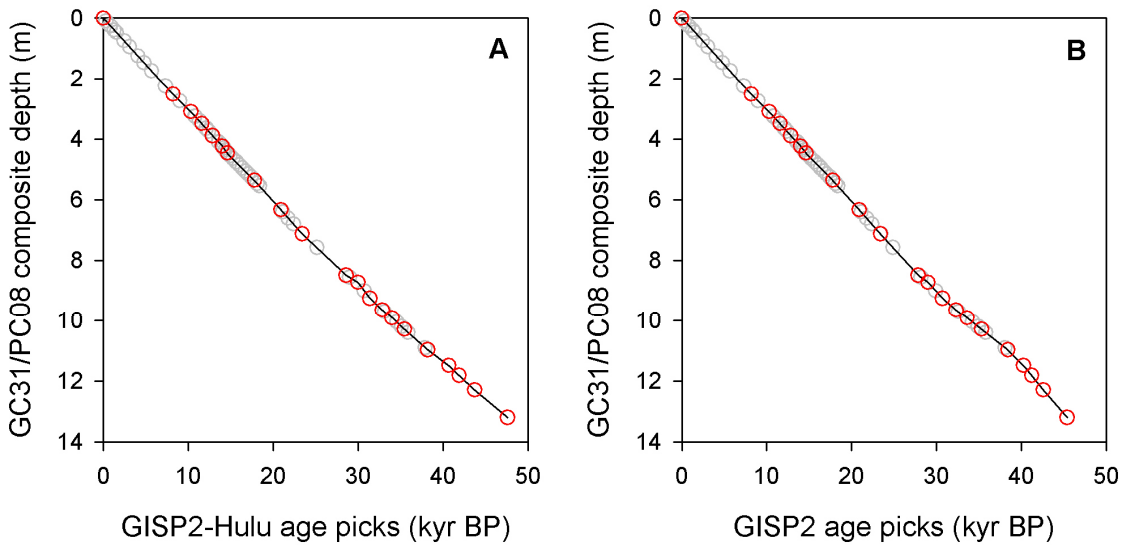

Fig. S2. (**A**) Age-depth relationship for MV99-MC19/GC31/PC08 based on correlation to GISP2 $\delta^{18}O$ with Hulu Cave age adjustment. Red points are tie-points and gray points represent radiocarbon measurements. The unusually constant sedimentation rate allows for relatively precise calendar age assignments between tie-points. (**B**) Same as (**A**) except using alternate age model as in Fig. S3.

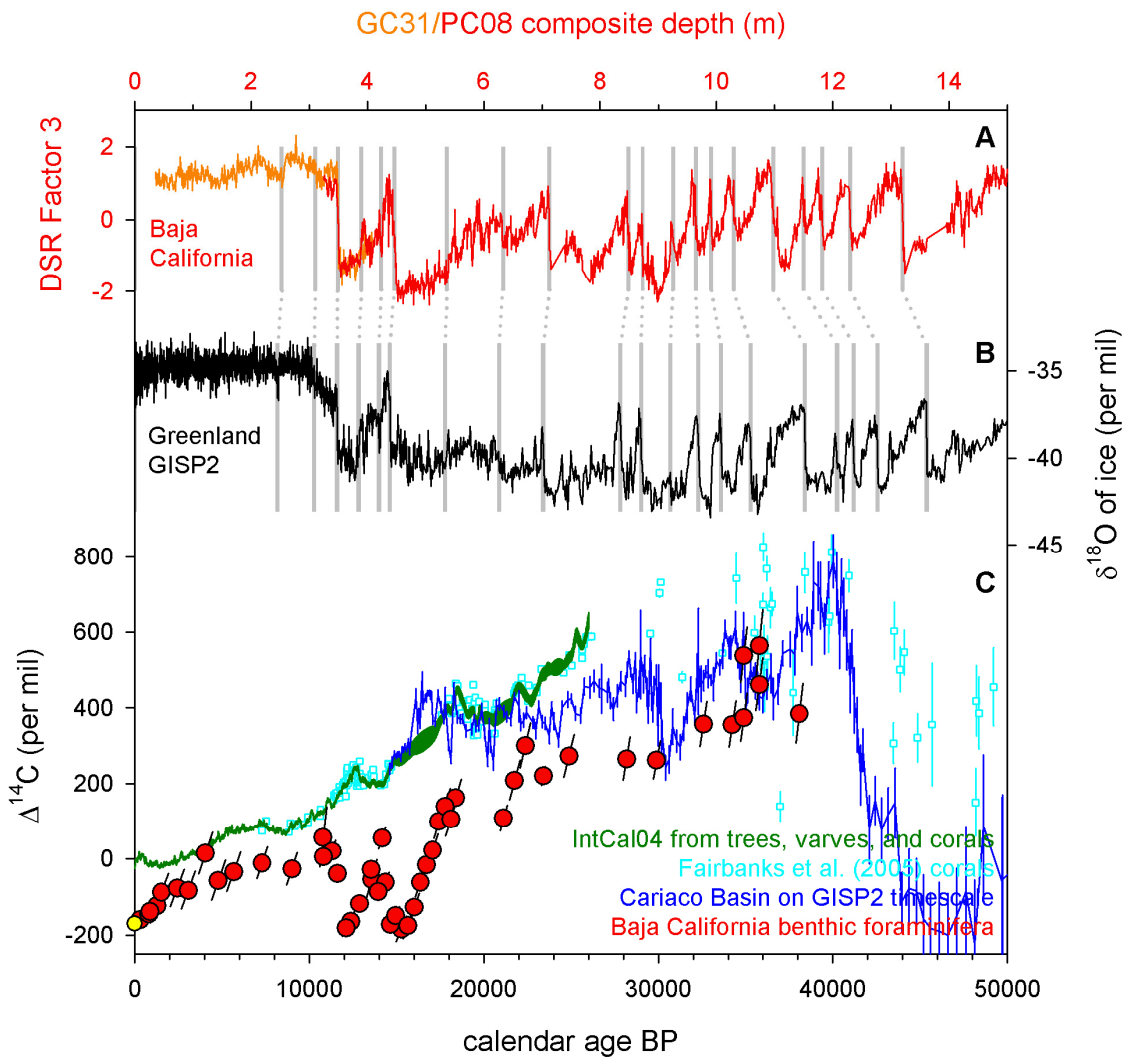

Fig. S3. Baja California $\Delta^{14}C$ record based on alternate age model. (**A**) Diffuse spectral reflectance factor 3 from Baja California composite sediment core MV99-GC31/PC08, plotted versus depth (top axis) (*S15*). Gray lines show tie-points to Greenland record used to derive alternate calendar age model. (**B**) $\delta^{18}O$ of Greenland ice core GISP2 on original timescale (bottom axis) (*S6, S16*). (**C**) Atmospheric radiocarbon activities based on tree rings, planktonic foraminifera from Cariaco Basin varve-counted sediments, and U-Th-dated corals (dark green) (*S3*); additional recent coral measurements (cyan) (*S4*); and planktonic foraminifera from Cariaco Basin using age model derived from reflectance correlation to GISP2 (blue) (*S17*). Red points show intermediate water activities from benthic foraminifera in MC19/GC31/PC08. Yellow point is estimate for modern bottom waters at this site.

Table S1. Core MC19/GC31/PC08 radiocarbon data.

Sample	Taxa	Composite depth (m)	^{14}C age (kyr BP)	^{14}C age error (kyr)	Calendar age (kyr BP)	Calendar age error (kyr)	$\Delta^{14}C$ (per mil)	$\delta^{13}C$ (per mil)	Accession #	Son?	Reference
MC19-10 cm	mixed benthics	0.100	1.720	0.030	0.32	0.1	-161	-0.61	OS-33198	no	*1*
MC19-25 cm	mixed benthics	0.250	2.050	0.035	0.81	0.2	-146	-0.69	OS-33199	no	*1*
GC31-3-2 cm	mixed benthics	0.270	2.050	0.030	0.87	0.3	-139	-0.86	OS-33201	no	*1*
MC19-40 cm	mixed benthics	0.400	2.320	0.035	1.29	0.4	-124	-0.56	OS-33200	no	*1*
GC31-3-22.5 cm	mixed benthics	0.475	2.230	0.035	1.54	0.4	-88	-0.91	OS-25612	no	*1*
GC31-3-50.5 cm	*Bolivina* spp.	0.755	3.030	0.040	2.44	0.4	-78	nm	OS-22946	no	*1*
GC31-3-70 cm	mixed benthics	0.950	3.690	0.045	3.08	0.4	-84	-0.60	OS-33202	no	*1*
GC31-3-100.5 cm	*Bolivina* spp.	1.255	3.840	0.050	4.07	0.4	14	nm	OS-22947	no	*1*
GC31-3-123 cm	mixed benthics	1.480	5.130	0.060	4.79	0.4	-57	-0.53	OS-33203	no	*1*
GC31-2-0.5 cm	*Bolivina* spp.	1.755	5.810	0.040	5.69	0.4	-35	nm	OS-22948	no	*1*
GC31-2-50.5 cm	*Bolivina* spp.	2.255	7.190	0.050	7.31	0.3	-11	nm	OS-22949	no	*1*
GC31-2-100.5 cm	*Bolivina* spp.	2.755	8.980	0.060	9.01	0.3	-27	-0.90	OS-22955	no	*1*
GC31-1-8.5 cm	*Bolivina* spp.	3.255	10.050	0.410	10.79	0.2	56	-1.15	OS-23513	no	*1*
PC08-9-45 cm	mixed benthics	3.260	10.460	0.030	10.81	0.2	6		CURL-8750	yes	this study
PC08-9-60 cm	mixed benthics	3.410	10.845	0.030	11.32	0.2	20		CURL-8752	yes	this study
GC31-1-32.5 cm	mixed benthics	3.495	11.600	0.070	11.61	0.1	-39	-1.49	OS-25611	no	*1*
PC08-9-85 cm	mixed benthics	3.660	13.380	0.035	12.12	0.2	-181		CURL-8751	yes	this study
GC31-1-58.5 cm	*Bolivina* spp.	3.755	13.500	0.070	12.41	0.2	-164	-1.49	OS-22956	no	*1*
PC08-9-110 cm	mixed benthics	3.910	13.530	0.030	12.88	0.1	-118		CURL-8444	no	this study
PC08-9-130 cm	mixed benthics	4.110	13.420	0.025	13.57	0.1	-29		CURL-8445	no	this study
GC31-1-94.5 cm	*Bolivina* spp.	4.115	13.650	0.150	13.58	0.3	-54	-1.43	OS-22957	no	*1*
PC08-9-141 cm	*Uvigerina* spp.	4.220	14.285	0.035	13.94	0.1	-88		CURL-8746	yes	this study
PC08-9-150 cm	mixed benthics	4.310	13.370	0.030	14.20	0.2	55		CURL-8446	no	this study
PC08-8-6.5 cm	*Uvigerina* spp.	4.375	14.485	0.035	14.37	0.2	-62		CURL-8721	yes	this study
PC08-8-16.5 cm	*Uvigerina* spp.	4.475	15.755	0.040	14.65	0.1	-172		CURL-8726	yes	this study
PC08-8-25.5 cm	*Uvigerina* spp.	4.565	15.850	0.040	14.96	0.2	-150		CURL-8720	yes	this study
PC08-8-35 cm	mixed benthics	4.660	16.505	0.040	15.30	0.3	-184		CURL-8447	no	this study

PC08-8-45.5 cm	*Uvigerina* spp.	4.765	16.785	0.045	15.67	0.3	-176		CURL-8724	yes	this study
PC08-8-55.5 cm	*Uvigerina* spp.	4.865	16.665	0.040	16.02	0.3	-127		CURL-8729	yes	this study
PC08-8-65.5 cm	*Uvigerina* spp.	4.965	16.425	0.045	16.37	0.3	-62		CURL-8744	yes	this study
PC08-8-75.5 cm	*Uvigerina* spp.	5.065	16.390	0.040	16.73	0.3	-17		CURL-8742	yes	this study
PC08-8-85.5 cm	*Uvigerina* spp.	5.165	16.425	0.050	17.08	0.3	22		CURL-8743	yes	this study
PC08-8-95.5 cm	*Uvigerina* spp.	5.265	16.185	0.045	17.43	0.3	98		CURL-8749	yes	this study
PC08-8-105.5 cm	*Uvigerina* spp.	5.365	16.235	0.040	17.78	0.3	139		CURL-8748	yes	this study
PC08-8-116 cm	*Uvigerina* spp.	5.470	16.810	0.040	18.12	0.3	105		CURL-8745	yes	this study
PC08-8-125 cm	mixed benthics	5.560	16.680	0.040	18.41	0.3	162		CURL-8448	no	this study
PC08-7-60.5 cm	*Uvigerina* spp.	6.415	19.720	0.060	21.14	0.2	108		CURL-8728	yes	this study
PC08-7-80.5 cm	*Uvigerina* spp.	6.615	19.640	0.060	21.77	0.3	208		CURL-8722	yes	this study
PC08-7-99.75 cm	mixed benthics	6.808	19.650	0.080	22.39	0.3	299	-0.81	OS-33204	no	*1*
PC08-7-132.5 cm	*Uvigerina* spp.	7.135	21.170	0.070	23.43	0.1	220		CURL-8727	yes	this study
PC08-6-20.5 cm	*Uvigerina* spp.	7.585	22.260	0.070	25.15	0.3	311		CURL-8725	yes	this study
PC08-6-118 cm	mixed benthics	8.560	25.500	0.170	29.00	0.2	396	-0.57	OS-33205	no	*1*
PC08-5-25 cm	mixed benthics	9.010	27.200	0.130	30.73	0.2	394		CURL-8449	no	this study
PC08-5-95 cm	mixed benthics	9.710	29.230	0.160	33.11	0.2	443		CURL-8450	no	this study
PC08-5-130 cm	*Uvigerina* spp.	10.060	30.830	0.170	34.55	0.2	407		CURL-7188	no	this study
PC08-5-145 cm	*Uvigerina* spp.	10.210	30.460	0.190	35.11	0.2	577		CURL-7189	no	this study
PC08-5-145 cm	*Bolivina* spp.	10.210	31.370	0.180	35.11	0.2	408		CURL-7192	no	this study
PC08-4-15 cm	mixed benthics	10.410	31.200	0.280	35.89	0.2	582	-0.72	OS-33206	no	*1*
PC08-4-15 cm	*Uvigerina* spp.	10.410	31.750	0.190	35.89	0.2	477		CURL-7187	no	this study
PC08-4-65 cm	*Bolivina* spp.	10.910	34.400	0.260	37.92	0.2	356		CURL-7193	no	this study

Composite depth is relative to the top of MC19, as in (*S1*). Calendar age errors are based on estimated precision of tie-points and distance of samples from tie-points. $\delta^{13}C$ data are only reported for NOSAMS measurements; 'nm' indicates not measured. Column labeled 'Son?' indicates whether or not radiocarbon samples were sonicated in methanol prior to graphitization.

Table S2. Tie-points between the EPICA Dome C EDC3 and GISP2 time scales.

EDC3 gas age (yr BP)	GISP2 gas age (yr BP)	estimated uncertainty (yr)	event description
0	0	0	
8200	8200	25	8.2 ka BP event
11400	11620	25	YD termination
12400	12750	100	Onset of YD
14110	14810	150	Onset of B-A
16700	17600	200	First deglacial CH_4 rise
21860	22950	300	CH_4 peak in GRIP and Dome C

SOM References

S1. A. van Geen *et al.*, *Paleoceanography* **18**, doi:10.1029/2003PA000911 (2003).
S2. M. Stuiver, H. A. Polach, *Radiocarbon* **19**, 355 (1977).
S3. P. J. Reimer, et al., *Radiocarbon* **46**, 1029 (2004).
S4. R. G. Fairbanks *et al.*, *Quaternary Science Reviews* **24**, 1781 (2005).
S5. K. Hughen, J. Southon, S. J. Lehman, C. Bertrand, J. Turnbull, *Quaternary Science Reviews*, **25**, 3216 (2006).
S6. P. M. Grootes, M. Stuiver, *Journal of Geophysical Research* **102**, 26455 (1997).
S7. Y. J. Wang *et al.*, *Science* **294**, 2345 (2001).
S8. A. Svensson *et al.*, *Quaternary Science Reviews*, **25**, 3258 (2006).
S9. E. Monnin *et al.*, *Science* **291**, 112 (2001).
S10. T. Blunier, E. Brook, *Science* **291**, 109 (2001).
S11. J. Flückiger *et al.*, *Global Biogeochemical Cycles* **16**, 1010 (2002).
S12. F. Parrenin *et al.*, *Climate of the Past Discussions* **3**, 19 (2007).
S13. L. Loulergue *et al.*, *Climate of the Past Discussions* **3**, 425 (2007).
S14. W. E. Dean, Y. Zheng, J. D. Ortiz, A. van Geen, *Paleoceanography* **21**, doi:10.1029/2005PA001239 (2006).
S15. J. D. Ortiz *et al.*, *Geology* **32**, 521 (2004).
S16. D. A. Meese *et al.*, *Journal of Geophysical Research* **102**, 26411 (1997).
S17. K. Hughen *et al.*, *Science* **303**, 202 (2004).

Brudzinski *et al.* have now found a direct correlation whereby older oceanic plates show a greater distance between regions of seismicity. They conclude, based on thermal-petrological models developed by Hacker *et al*. (*5*), that dehydration of the mineral antigorite is responsible for the seismicity in the lower layer of double WBZs.

Although the detailed geophysical explanation presented by Brudzinski *et al*. for the double seismic zone might be debatable, they observe that double WBZs are the rule and not the exception during subduction of oceanic lithosphere. This provides an important new constraint for all models developed to explain the occurrence of WBZ seismicity. However, further work on the stress accumulation and dissipation in the lithosphere during subduction is necessary to understand the faulting mechanism causing seismicity in double WBZ or even triple WBZ, as proposed for some regions beneath Japan (*6*).

Brudzinski *et al.* show that, as the number of seismological stations and the availability of digital seismic traces increases, the global earthquake catalog will become accurate enough to delineate the fine structure of seismicity (on the order of a few kilometers) on a global scale. This accuracy will increase in the near future as a result of large seismological observation initiatives like EarthScope in the United States or the NERIES program (Network of Research Infrastructures for European Seismology) in Europe, which will make more high-quality digital data readily available for seismologists worldwide.

References

1. M. R. Brudzinski, C. H. Thurber, B. R. Hacker, E. R. Engdahl, *Science* **316**, 1472 (2007).
2. A. Hasegawa, N. Umino, A. Takagi, *Tectonophysics* **47**, 43 (1978).
3. A. Rietbrock, F. Waldhauser, *Geophys. Res. Lett.* **31**, 10.1029/2004GL019610 (2004).
4. S. Kirby, *Rev. Geophys.* **33,** 287 (1995).
5. B. R. Hacker, G. A. Abers, S. M. Peacock, *J. Geophys. Res*. **108**, 2029 (2003).
6. T. Igarashi, T. Matsuzawa, N. Umino, A. Hasegawa, *J. Geophys. Res.* **106**, 2177 (2001).

10.1126/science.1141921

ATMOSPHERE

Deglaciation Mysteries

Results from a sediment core provide insights into ocean circulation changes during the last deglaciation.

Ralph F. Keeling

Between 19,000 and 11,000 years ago, the Earth emerged from the last glacial period. During this deglaciation, the carbon dioxide (CO_2) concentration in the atmosphere rose from 180 to 265 parts per million (ppm). Over the same period, the radiocarbon content of the CO_2 fell by ~35%. A simple but unproven explanation for both changes is an increase in the rate at which the ocean's subsurface waters were renewed by exchange with aerated surface waters—a process known as ventilation. A ventilation increase could increase atmospheric CO_2 concentration by releasing excess CO_2 that had accumulated in subsurface waters by the decomposition of sinking detritus. On page 1456 in this issue, Marchitto *et al.* (*1*) bolster the case for such a ventilation increase and offer insight into how the increase may have occurred.

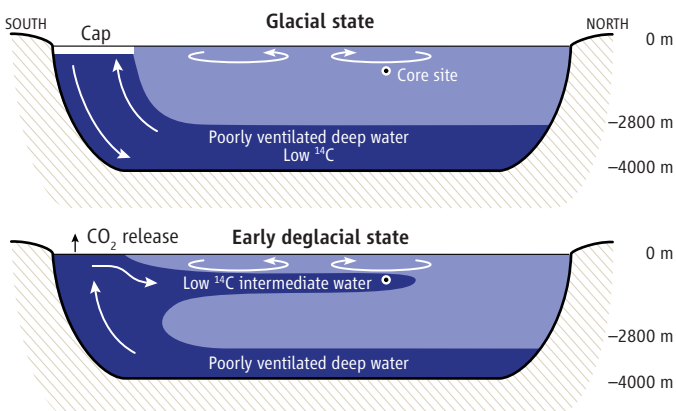

Deep-water ventilation. This cross section of the Pacific Ocean shows how poorly ventilated water may have been delivered to intermediate depths during deglaciation, as suggested by Marchitto *et al*. (**Top**) Ventilation of the deep ocean by sinking around Antarctica was partially suppressed by a cap formed by sea ice or a layer of low-salinity water. (**Bottom**) This cap was removed during early deglacial warming, exposing upwelled deep waters to the atmosphere, releasing radiocarbon-depleted CO_2. The density of the poorly ventilated waters was reduced by freshening and warming. With reduced density, the water could spread widely at intermediate depths, displacing waters of similar density.

To track changes in past ventilation, most researchers have turned to measurements of the radiocarbon (^{14}C) content of shells of foraminifera, a ubiquitous marine microorganism. Radiocarbon is produced naturally in the upper atmosphere by cosmic rays and spreads through the ocean as part of the pool of dissolved carbon. Because of radioactive decay, waters that are more isolated from the atmosphere (that is, more poorly ventilated) have lower $^{14}C/^{12}C$ ratios, as do the shells that grow in these waters. The radiocarbon age of a fossil shell therefore reflects the age of the shell plus the age of the water in which it lived. By subtracting the radiocarbon ages of surface-dwelling (planktonic) and bottom-dwelling (benthic) foraminifera, picked from the same layer of a sediment core, it is possible to estimate age difference of surface and deep waters, which is a measure of the deep-water ventilation rate.

This technique, applied to numerous sediment cores, has thus far mainly yielded the unremarkable result that the ventilation rate of the glacial ocean was very similar to that of today's ocean, at least down to a depth of ~2800 m (*2*). Thus, if there was a major change in ocean ventilation during deglaciation, this change must have occurred in ocean waters below that depth. However, despite some tantalizing results (*3*), no general picture has emerged for waters below 2800 m, because of methodological difficulties related to the low sedimentation rates that typically characterize cores from these depths.

Marchitto *et al.* focus on a sediment core recently hauled up off Baja California from a depth of 700 m, seemingly too shallow for studying deep ventilation. The core contains bands corresponding to a set of millennial climate oscillations first discovered in ice cores from Greenland, allowing absolute dates to be fixed within the core. Using these dates, the authors correct the $^{14}C/^{12}C$ ratios of benthic foraminifera for radioactive decay, thus establishing the original $^{14}C/^{12}C$ ratio of the water in which the foraminifera lived. The technique does not require $^{14}C/^{12}C$ measurements on planktonic

The author is at the Scripps Institution of Oceanography, University of California, San Diego, CA 92093, USA. E-mail: rkeeling@ucsd.edu

Downloaded from www.sciencemag.org on June 7, 2007

Published by AAAS

foraminifera, which are subject to potentially large systematic errors.

The results show two periods during deglaciation when the bottom water at their site had unexpectedly low $^{14}C/^{12}C$ ratios. The water was so old that it must have been delivered to the site by upwelling from greater depth, presumably from below 2800 m. The oldest waters found by Marchitto *et al.* have an age of ~4000 years. For comparison, the oldest waters in the modern ocean have an age of ~2300 years.

The study provides the strongest evidence to date that the glacial ocean contained some very poorly ventilated water somewhere in its depths. The low-^{14}C periods coincide with the periods when atmospheric radiocarbon decreased and atmospheric CO_2 increased most rapidly during deglaciation. The results are thus a convincing fingerprint of a process that flushed excess carbon from an isolated deep reservoir toward the surface, thereby driving the atmospheric changes.

Today, waters below 2800 m are ventilated by two routes. One involves the sinking of aerated surface waters in the North Atlantic, the other sinking of such waters near Antarctica. During the last glacial period, both routes probably weakened, with the southern route possibly influenced by sea ice or surface freshening (see the figure, top panel). During glacial times, the deep ocean would thus have been less ventilated than it is today.

But how could low-^{14}C waters get to Marchitto *et al.*'s core site during deglaciation? Much of the upwelling of deep water occurs today around Antarctica, resulting in the formation of Antarctic Intermediate Water, a low-salinity water mass that spreads northward at intermediate depths. Marchitto *et al.* hypothesize that a similar process occurred during deglaciation, allowing upwelled water to spread northward to their site (see the figure, bottom panel). However, the evidence for this southern pathway is circumstantial.

The results help to reconcile the reconstructed trends in atmospheric radiocarbon with the estimated trends in the production of radiocarbon by cosmic rays—a comparison that seems to demand an increase in ocean ventilation during deglaciation (*4*). They support theories that attribute the bulk of the glacial-interglacial CO_2 change to changes in ocean ventilation (*5*, *6*).

The study also provides support for a theory for how the glacial ocean differed from today's ocean as a result of the cooling of deep waters to nearly the freezing point. Cooling to this extent is expected to allow the salty brine that is released during sea ice formation to accumulate more easily in the deep ocean (*7*). This idea is supported by sediment pore-water studies (*8*). By blocking the input of fresh water from precipitation, sea ice could also reduce the conversion of upwelled deep water into low-salinity Antarctic Intermediate Water (*7*). A strengthening of intermediate-water formation during deglaciation is consistent with a breakdown of this state caused by warming.

The study nevertheless leaves the skeptics with arrows in their quiver. Marchitto *et al.*'s low-^{14}C waters are so old that they start to stretch credibility, especially considering that the deep reservoir from which the water was drawn must have been even older. (This follows because some mixing with younger water would unavoidably have occurred during upwelling and transit to the site.) How could prior studies have overlooked deep waters this old?

If Marchitto *et al.*'s interpretation is correct, evidence for old water at intermediate depths should be present throughout the South Pacific in sediments of the appropriate age and depth. If subsequent work supports the findings, we may look back at this study as a key turning point in the quest to understand glacial and interglacial CO_2 changes.

References

1. T. M. Marchitto, S. J. Lehman, J. D. Ortiz, J. Flückiger, A. van Geen, *Science* **316**, 1456 (2007); published online 10 May 2007 (10.1126/science. 1138679).
2. W. Broecker *et al.*, *Paleoceanography* **22**, PA2206 (2007).
3. L. D. Keigwin, S. J. Lehman, M. S. Cook, *Eos* **87**, PP44A07 (2006).
4. K. Hughen *et al.*, *Science* **303**, 202 (2004).
5. J. R. Toggweiler, J. L. Russell, S. R. Carson, *Paleoceanography* **21**, PA2005 (2006).
6. B. B. Stephens, R. F. Keeling, *Nature* **404**, 171 (2000).
7. R. F. Keeling, B. B. Stephens, *Paleoceanography* **16**, 112 330 (2001).
8. J. F. Adkins, K. McIntyre, D. P. Schrag, *Science* **298**, 1769 (2002).

Published online 10 May 2007;
10.1126/science.1142326.
Include this information when citing this paper.

Downloaded from www.sciencemag.org on June 7, 2007

MOLECULAR BIOLOGY

Site-Seeing by Sequencing

Stanley Fields

An advance in DNA sequencing is a crucial component of a rapid, precise, and relatively inexpensive way to identify transcription factor binding sites at a whole-genome level.

Every few years, a new technology comes along that dramatically changes how fundamental questions in biology are addressed. The impact of the technology is not always appreciated at first—when it is used only by those involved in its development—but becomes clear once the technology begins to spread to the broader scientific community. A well-known example is the DNA microarray, which became widely available to biologists about a decade ago and has since been applied to an ever-expanding set of questions such as determining the profile of genes expressed in a specific cell type. Now it is ultrahigh-throughput DNA sequencing that is making the transition from development to widespread use. Johnson and colleagues are in the vanguard of this movement. On page 1497 of this issue (*1*), they report that an advanced DNA sequencing technology (from Solexa/Illumina) can be used to identify all the locations in the human genome where a specific protein binds. They do this with a speed and precision that goes beyond what has been achieved with previous technologies.

DNA-binding proteins control transcription, replication, DNA repair, and chromosome segregation. Given the importance of these proteins, identifying their binding sites throughout the genome has occupied much attention in recent years. The most common method of locating these sites within a living cell is known as chromatin immunoprecipitation (ChIP). In this approach, cells are treated with a reagent, typically formaldehyde, that crosslinks protein and DNA, and then the cells are lysed. Chromatin (the complex of proteins and DNA in chromosomes) is isolated, the DNA is sheared into small fragments, and an antibody is added to precipitate the protein and its associated DNA. The DNA that is liberated after reversal of the protein-DNA crosslinks is then analyzed. In the initial uses of this method, researchers analyzed the DNA to determine whether single genes were enriched by the immunoprecipitation.

The author is in the Departments of Genome Sciences and Medicine, Howard Hughes Medical Institute, University of Washington, Seattle, WA 98195–5065, USA. E-mail: fields@u.washington.edu

Published by AAAS